Journal of Solid State Chemistry **144,** 169–174 (1999)
Article ID jssc.1999.8141, available online at http://www.idealibrary.com on IDEAL®

Structure Characterization and Magnetic Behavior of $NaNi_4(PO_4)_3$ and $KMn_4(PO_4)_3$

Abdelaali Daidouh,*,[1] J. L. Martinez,† C. Pico,* and M. L. Veiga*

*Departamento Química Inorgánica I, Facultad de Ciencias Químicas, Universidad Complutense, 28040 Madrid, Spain; and
†Instituto de Ciencias de Materiales, CSIC, Cantoblanco, E-28049 Madrid, Spain

Received August 4, 1998; in revised form December 16, 1998; accepted January 5, 1999

New sodium nickel and potassium manganese orthophosphates $NaNi_4(PO_4)_3$ (abbreviated as *NNP*) and $KMn_4(PO_4)_3$ (*KMP*) with tunnel structures have been synthesized. They crystallizes in the orthorhombic space group Pnmm with $a = 6.148(6)$ Å, $b = 16.210(1)$ Å, $c = 9.479(4)$ Å for (*NNP*), and $a = 6.554(8)$ Å, $b = 16.04(9)$ Å, $c = 9.977(2)$ Å for (*KMP*). The structure is built up from trinuclear groups of edge-sharing MO_6 octahedra, giving rise to the $[M_3O_{11}]_\infty$ chains running along the [100] direction. Both materials show antiferromagnetic interactions and exhibit spontaneous magnetization at low temperatures, which can be explained by a canting of spin arrangement, giving rise to a weak ferromagnetic component. This behavior can be interpreted on the basis of structural features and the characteristics of single-ion intercalations.

INTRODUCTION

Compounds with covalent networks built up from XO_4 tetrahedra (X = Si, P, Ge, As) and MO_6 octahedra are extensively studied, because they offer interesting examples of materials exhibiting fast-alkali-ion mobility and ion-exchange properties (1–5). Indeed, when M is a divalent-transition metal, different magnetic behaviors have been observed (6, 7).

This paper reports on two new orthophosphates, $NaNi_4(PO_4)_3$ and $KMn_4(PO_4)_3$, abbreviated *NNP* and *KMP*, respectively, whose structures were found to be isostructural to those of $KFe_4(PO_4)_3$ and $RbMn_4(AsO_4)_3$ (8, 9). The connectivity of the octahedral tetrahedral units in title metal phosphates results in six-sided windows, giving rise to channels running along the [100] direction where the alkali cations are located, which suggests an ionic mobility in the compounds. The ionic conductivity properties are under study (10) and will be soon published. At the same time, the structure exhibits an interesting $[M_3O_{11}]_\infty$ chains formed by three octahedral MO_6 units (Ni^{2+}/Mn^{2+}) sharing edges, which suggests in turn that magnetic interactions between spins could take place. The magnetic behaviors are discussed from structural- and single-ion characteristics.

[1] To whom correspondence should be addressed.

EXPERIMENTAL

The title compounds were prepared using a sol–gel method in aqueous solutions, starting from stoichiometric proportions of $NaNO_3$ and $Ni(NO_3)_2.6H_2O$ for *NNP* or KNO_3 and $C_{10}H_{14}MnO_4$ for *KMP*, as well as $(NH_4)_2HPO_4$ in both cases. The solutions were dried overnight at 373 K giving rise to gelatinous precipitates. These gels were heated at different temperatures ranging from 623 to 1073 K with intervening mixing and grinding. The resulting powders (yellow for *NNP* and white for *KMP*) were subsequently identified as pure phase by X-ray diffraction.

X-ray diffraction patterns were collected with a Philips X'Pert MPD powder diffractometer. CuKα radiation was used and filtered with a graphite monochromator in the angular range $10^\circ < 2\theta < 100^\circ$ using a counting time of 12 s for each step. The selected profiles were refined by Rietveld's method (11).

Magnetic properties were measured with a SQUID magnetometer. The temperature dependence of susceptibilities was registered at decreasing temperatures from 300 to 2 K at an applied field of 0.5 T.

RESULTS AND DISCUSSION

Structure Description

The structures of $NaNi_4(PO_4)_3$ and $KMn_4(PO_4)_3$ have been determined by X-ray powder diffraction using the Rietveld refinement, starting from the isostructural phase $KFe_4(PO_4)_3$ (8). The final results of this refinement are presented in Tables 1, (for the unit cell parameters), 2, 3 (for the atomic positions), 4, and 5 (for the interatomic distances). An example of the observed, calculated and difference patterns are given in Fig. 1 (for *NNP*).

0022-4596/99 $30.00

TABLE 1
Summary of Structure Parameters for $NaNi_4(PO_4)_3$ and $KMn_4(PO_4)_3$ (Rietveld Refinement Data)

	$NaNi_4(PO_4)_3$	$KMn_4(PO_4)_3$
1. Structure Parameters		
Space group	*Pmnn*	*Pmnn*
a (Å)	6.148(6)	6.554(8)
b (Å)	16.210(1)	16.049(5)
c (Å)	9.479(4)	9.977(2)
V (Å^3)	944.80(1)	1049.61(4)
2. Structure solution and Refinement		
R_P	11.4	13.9
R_{WP}	14.7	17.0
R_B	6.52	8.52
χ^2	8.13	5.40
Refined parameters	58	58
Reflections	1556	1728

The projection of the structure in the *ab* plane (Fig. 2) shows its complexity, that can be rationalized as made up by $[M_4P_3O_{12}]_\infty$ sheets parallel to the (001) plane and giving raise to tunnels, where the alkali cations are located. A triangular $[M_3O_{13}]$ basal unit is built by the edge linkages of three MO_6 octahedra, as is depicted separately in Fig. 3. Such a unit is formed by two kinds of transition-metal cations, two labeled as $M(3)$, which are in general positions, that share opposite edges forming linear $[M(3)O_8]_\infty$ chains, and one $M(2)$ sharing one edge with each $M(3)O_6$ pair. In the same manner, a tetrahedron $P(2)O_4$ is connected to this triangular unit, in the opposite side of $M(2)O_6$, via common edges to two $M(3)O_6$ octahedra. It results in $[M_3PO_{12}]_\infty$ columns running along the [100] direction as is clearly showed in Fig. 3.

TABLE 2
$NaNi_4(PO_4)_3$ Positional Parameters

Atom	Position	x/a	y/b	z/c
Na	4*g*	0.5	0.030(7)	0.797(9)
Ni(1)	4*g*	0	0.092(08)	0.535(2)
Ni(2)	4*g*	0	0.141(5)	0.984(7)
Ni(3)	8*h*	0.251(7)	0.204(5)	0.248(5)
P(1)	4*g*	0.5	0.161(1)	0.542(08)
P(2)	4*g*	0.5	0.219(7)	0.952(4)
P(3)	4*g*	0	0.034(2)	0.205(7)
O(1)	4*g*	0.5	0.174(1)	0.383(8)
O(2)	4*g*	0.5	0.228(08)	0.116(08)
O(3)	8*h*	0.298(4)	0.114(2)	0.591(4)
O(4)	4*g*	0	0.187(4)	0.390(5)
O(5)	4*g*	0.5	0.248(9)	0.606(8)
O(6)	4*g*	0	0.045(8)	0.867(2)
O(7)	8*h*	0.201(1)	0.087(6)	0.158(6)
O(8)	8*h*	0.710(4)	0.177(08)	0.895(08)
O(9)	4*g*	0	0.019(4)	0.365(5)

TABLE 3
$KMn_4(PO_4)_3$ Positional Parameters

Atom	Position	x/a	y/b	z/c
K	4*g*	0.5	0.032(2)	0.761(6)
Mn(1)	4*g*	0	0.116(4)	0.551(4)
Mn(2)	4*g*	0	0.129(5)	0.976(8)
Mn(3)	8*h*	0.250(5)	0.199(6)	0.251(2)
P(1)	4*g*	0.5	0.179(4)	0.538(6)
P(2)	4*g*	0.5	0.214(4)	0.950(3)
P(3)	4*g*	0	0.036(2)	0.217(8)
O(1)	4*g*	0.5	0.201(4)	0.381(2)
O(2)	4*g*	0.5	0.220(4)	0.109(3)
O(3)	8*h*	0.310(4)	0.124(5)	0.573(1)
O(4)	4*g*	0	0.196(3)	0.392(5)
O(5)	4*g*	0.5	0.259(5)	0.623(5)
O(6)	4*g*	0	0.063(8)	0.800(4)
O(7)	8*h*	0.203(4)	0.073(6)	0.167(5)
O(8)	8*h*	0.701(3)	0.168(6)	0.902(3)
O(9)	4*g*	0	0.021(3)	0.370(3)

On the other hand, one can observe another type of chain of composition $[MPO_7]_\infty$, that is made up of $M(1)O_5$ square pyramids and $P(3)O_4$ tetrahedra associated by a common O(3), the unique oxygen atom which is only bicoordinated in the structure. Two parallel $[MPO_7]_\infty$ chains are interconnected in such a way that the square pyramids share one edge, giving rise to $[MPO_6]_\infty$ double chains (Fig. 4). The alkali cations, Na in *NNP* or K in *KMP*, are situated in the hexagonal windows formed by the above

TABLE 4
Interatomic and Mean Bond Distances for $NaNi_4(PO_4)_3$

Na–O(3) = 2.683(4) × 2	P(1)–O(1) = 1.513(7)
Na–O(7) = 2.687(5) × 2	P(1)–O(3) = 1.530(1) × 2
Na–O(8) = 2.864(7) × 2	P(1)–O(5) = 1.545(7)
P(2)–O(2) = 1.556(7)	P(3)–O(6) = 1.470(4)
P(2)–O(4) = 1.616(2)	P(3)–O(7) = 1.573(2) × 2
P(2)–O(8) = 1.559(2) × 2	P(3)–O(9) = 1.533(7)
Ni(1)–O(3) = 1.944(1) × 2	Ni(2)–O(5) = 2.120(4)
Ni(1)–O(4) = 2.067(1)	Ni(2)–O(6) = 1.909(8)
Ni(1)–O(9) = 1.993(2)	Ni(2)–O(7) = 2.240(3) × 2
Ni(1)–O(9) = 2.036(4)	Ni(2)–O(8) = 2.059(1) × 2
Ni(3)–O(1) = 2.053(9)	Ni(3)–O(5) = 2.184(2)
Ni(3)–O(2) = 2.013(3)	Ni(3)–O(7) = 2.099(8)
Ni(3)–O(4) = 2.069(8)	Ni(3)–O(8) = 2.373(4)

Mean bond distances[a] (Å)

Na–O	2.74	Ni(1)–O	1.99
P(1)–O	1.53	Ni(2)–O	2.10
P(2)–O	1.58	Ni(3)–O	2.13
P(3)–O	1.54		

[a] Shannon ionic radii sums (Å): $[NaO_6] = 2.42$; $[PO_4] = 1.57$; $[NiO_5] = 2.03$; $[NiO_6] = 2.09$.

TABLE 5
Interatomic Distances, Means, and Shannon Values for $KMn_4(PO_4)_3$

K–O(3) = 2.801(5) × 2	P(1)–O(1) = 1.608(8)
K–O(7) = 2.779(5) × 2	P(1)–O(3) = 1.559(7) × 2
K–O(8) = 2.909(3) × 2	P(1)–O(5) = 1.535(6)
P(2)–O(2) = 1.589(3)	P(3)–O(6) = 1.603(8)
P(2)–O(4) = 1.540(8)	P(3)–O(7) = 1.539(4) × 2
P(2)–O(8) = 1.585(7) × 2	P(3)–O(9) = 1.548(7)
Mn(1)–O(3) = 2.049(6) × 2	Mn(2)–O(5) = 2.305(3)
Mn(1)–O(4) = 2.033(4)	Mn(2)–O(6) = 2.057(3)
Mn(1)–O(9) = 2.366(5)	Mn(2)–O(7) = 2.494(6) × 2
Mn(1)–O(9) = 2.351(4)	Mn(2)–O(8) = 2.184(7) × 2
Mn(3)–O(1) = 2.090(5)	Mn(3)–O(5) = 2.181(3)
Mn(3)–O(2) = 2.188(3)	Mn(3)–O(7) = 2.222(7)
Mn(3)–O(4) = 2.166(9)	Mn(3)–O(8) = 2.622(9)

Mean bond distances[a] (Å)

K–O	2.82	Mn(1)–O	2.17
P(1)–O	1.55	Mn(2)–O	2.29
P(2)–O	1.57	Mn(3)–O	2.25
P(3)–O	1.56		

[a] Shannon ionic radii sums (A): $[KO_6]$ = 2.78; $[PO_4]$ = 1.57; $[MnO_5]$ = 2.15; $[MnO_6]$ = 2.23.

$[MPO_6]_\infty$ double chains, and the superposing windows originate tunnels running along the *c* axis.

Magnetic Behavior

The magnetization results for *NNP* and *KMP* are shown in Figs. 5 and 6, respectively, for the temperature range 300–2 K. The Curie–Weiss parameters obtained from least square fits of $H/M = (T - \theta)/C$, at $H = 0.5$ T, are gathered in Table 6. At lower temperatures the reciprocal susceptibility variation deviates from the Curie–Weiss law due to the onset of magnetic ordering.

Magnetization increases when temperature decreases, showing a transition at the Néel temperature, 20 K for *NNP* and 26 K for *KMP*, and reaching a sharp maximum at 8 and 16 K, respectively. The maximum value reached in the Ni compound (13.74 emu mol^{-1}) is much higher than that of the Mn (0.45 emu mol^{-1}). In the same sense, there is a significant increase of the $(M/H).T$ product for the Ni compound (186 K emu mol^{-1}) with respect to the Mn one (10.6 K emu mol^{-1}).

Taking into account first the moment variation obtained at high temperature, second the drop of the $(M/H).T$ product at low temperature, and finally the negative charge of

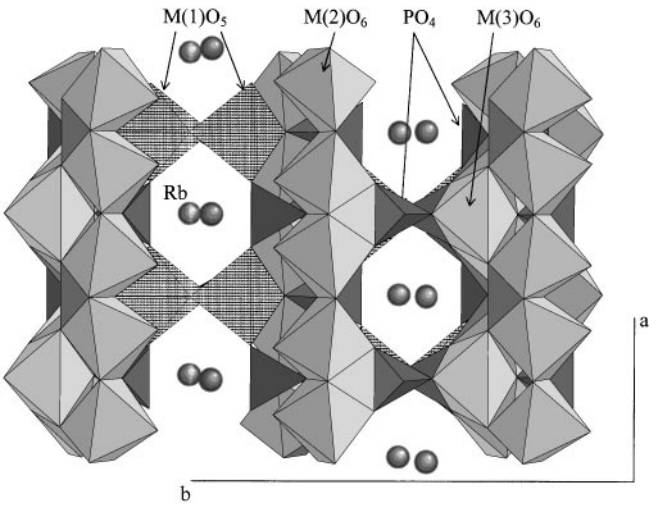

FIG. 2. Projection view along the [001] direction of the structure of $(NaNi_4/KMn_4)(PO_4)_3$ compounds.

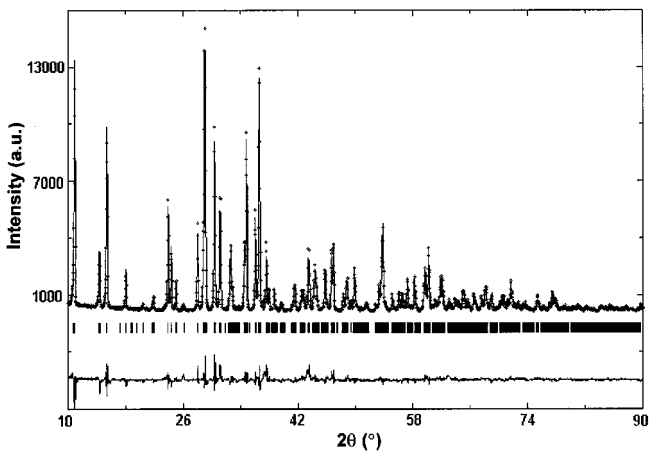

FIG. 1. Observed (crosses), calculated (solid line), and difference (bottom) X-ray powder diffraction patterns of $NaNi_4(PO_4)_3$ obtained from Rietveld's refinement.

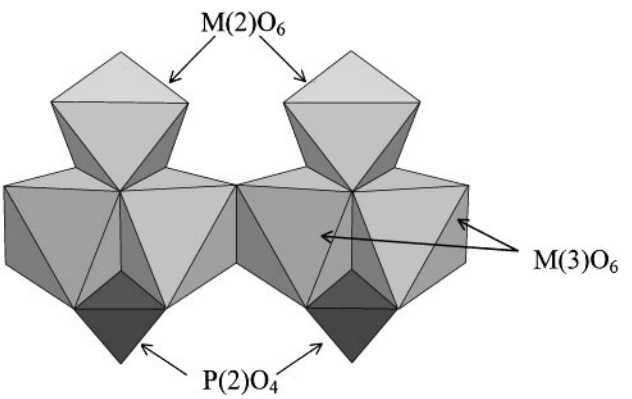

FIG. 3. Partial projection of the $[M_3PO_{12}]_\infty$ chains running along *a*, showing the $[M_3O_{13}]$ trinuclear groups.

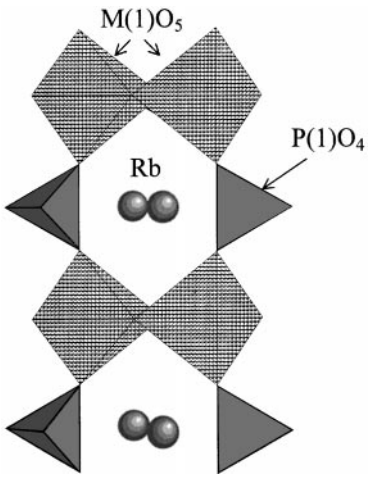

FIG. 4. Projection of the $[MPO_6]_\infty$ double chains along c.

the θ parameter, we can conclude that the dominant magnetic exchange interaction is antiferromagnetic in nature (12, 13). However, in both compounds the shift of the maxima in the magnetization below T_N can be attributed to a short-range magnetic ordering on a weakly ferromagnetic component (14–16). It may be noted that the ferromagnetic behavior is strongly marked in the nickel phosphate due to the higher maxima reached in the evolution of the above parameters with temperature, as well as its very low value of the Weiss temperature.

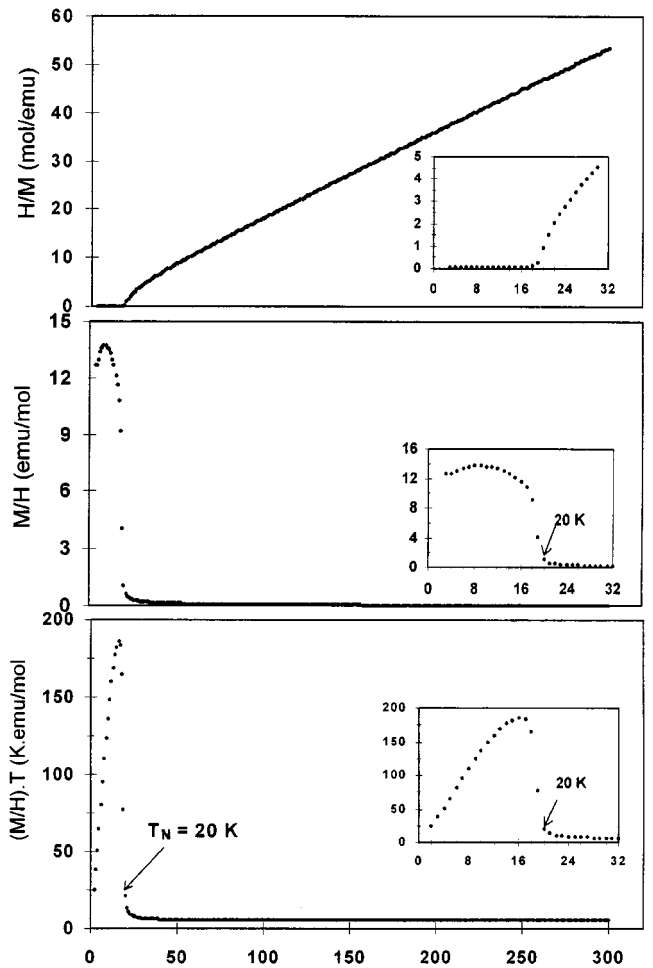

FIG. 5. Magnetic susceptibility data for $NaNi_4(PO_4)_3$ in an applied field of 500 G showing H/M, M/H, and $M/H{\cdot}T$ vs T.

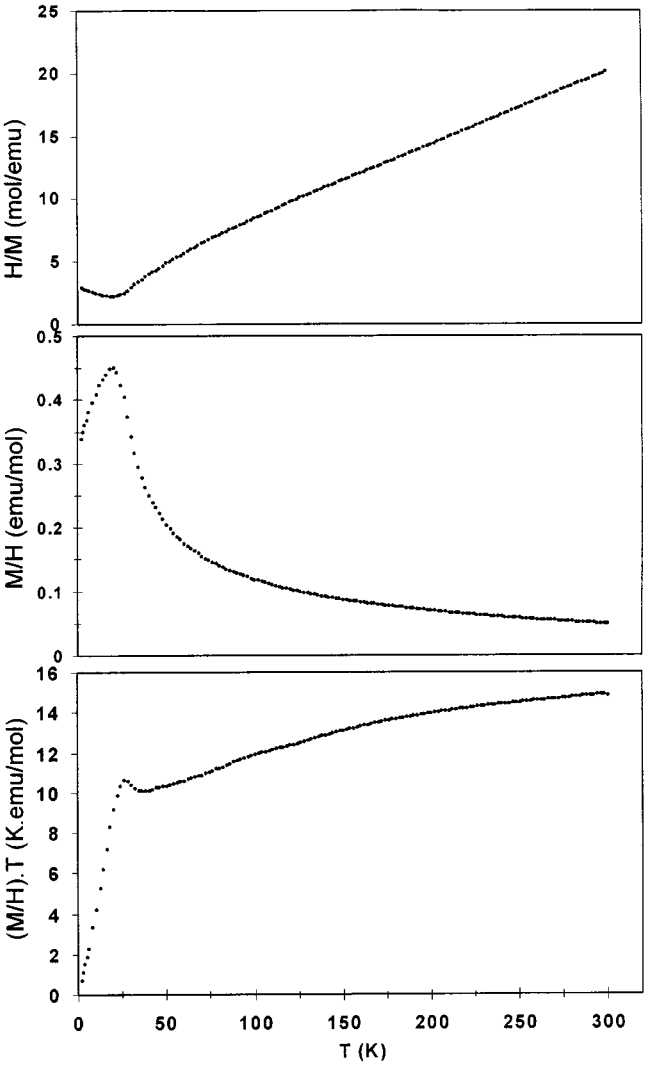

FIG. 6. Magnetic susceptibility data for $KMn_4(PO_4)_3$ in an applied field of 500 G showing $1/\chi_m$, χ_m and $\chi_m{\cdot}T$ vs T.

TABLE 6
Curie–Weiss Parameters for $NaNi_4(PO_4)_3$ and $KMn_4(PO_4)_3$

	C_m (emu K mol^{-1})	θ (K)	μ (μ_B)
$NaNi_4(PO_4)_3$	1.40	− 0.47	3.34
$KMni_4(PO_4)_3$	4.31	− 47.02	5.87

The peculiar magnetic behavior of both phosphates led us to undertake a more detailed study on the field-dependence magnetization at various temperatures. A ferromagnetically ordered component is clearly revealed by the observation of the hysteresis loops. The *NNP* compound showed rectangular loops at 2 and 14 K that disappear at 50 K (Fig. 7). The evaluation of this ferromagnetic component gives a value of $0.57\,\mu_B$ per Ni at atom 2 K, which is rather strong. In contrast, very low hysteresis loops are observed for the *KMP* compound at 2 and 25 K, these also disappear at 50 K (Fig. 8), and the ferromagnetic component is only $0.02\,\mu_B$ per Mn atom at 2 K.

A weakly ferromagnetism was demonstrated in a wide variety of phosphate and arsenate compounds (17–20), which usually is the result of a tilting of magnetic moments toward one another, giving rise to an inexact cancellation of antiferromagnetically ordered sublattices (21, 22).

The strong ferromagnetic behavior observed in the Ni compound, that is very weak in the Mn compound, can be presumably attributed to some structural differences between them. Although both phases are isostructural and they have similar polyhedra arrangements, the structure refinement shows that the *b* axis for *NNP* is somewhat longer (16.24 Å) than for *KMP* (16.04 Å), despite Mn^{2+} cations being larger than Ni^{2+} cations in the same octahedral coordination. This fact is also registered in the respective unit-cell volumes (cf. Table 1). Therefore, the octahedral groups forming $[M(3)_2O_8]_\infty$ chains along the *b* axis give rise to a zigzag configuration between these units (central common edge between $M(3)O_6$ pairs in Fig. 3, having in mind that inside these pairs the arrangement is more rigid due to the coordination of the $M(2)O_6$ octahedron and $P(2)O_4$ tetrahedron on both sides of the adjacent common edges). As much as the angle between $M(3)O_6$–$M(3)O_6$ octahedra is smaller along the zigzag chains, the respective *b* axis is shortened, giving rise to a higher tilting of the magnetic moments (23, 24). On the other hand, we can also consider other possible explanations of this behavior, more in the spirit of the magnetic interactions related to the single ion anisotropy. A single Ni^{2+} (d^8) ion has strong anisotropy, which could produce a strong ferromagnetic component in the structure along the imposed preferential direction. This fact is clearly different from an isotropic Mn^{2+} (d^5) system, which could not force the magnetic structure to impose a preferential direction. To confirm the validity of these hypotheses, the resolution of the magnetic structures by neutron powder diffraction is currently in progress.

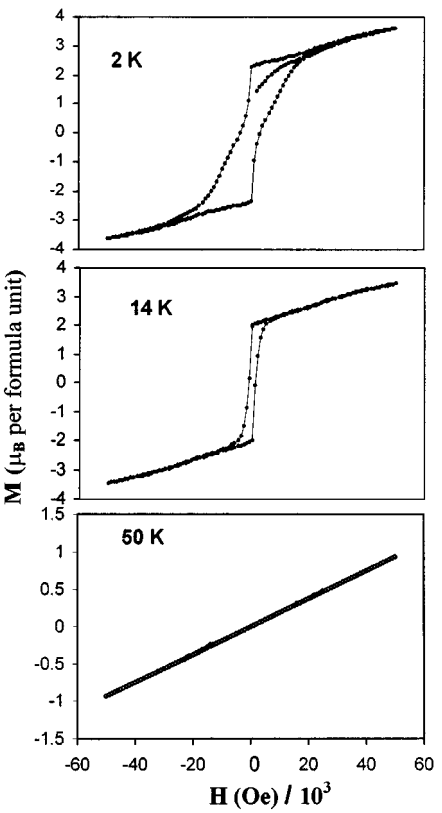

FIG. 7. Hysteresis measurements of $NaNi_4(PO_4)_3$ at 2, 14, and 50 K.

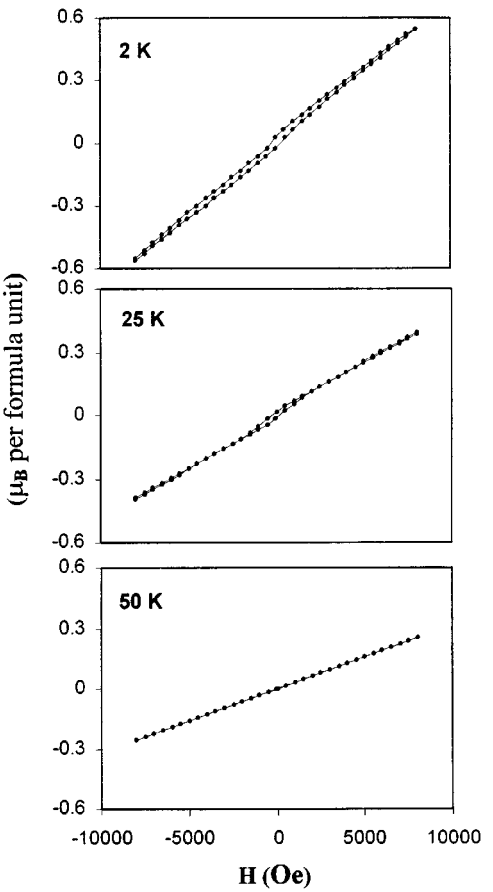

FIG. 8. Hysteresis measurements of $KMn_4(PO_4)_3$ at 2, 25, and 50 K.

ACKNOWLEDGMENT

We are indebted to the CICYT(MAT 97-0326-CO4-03) for financial support.

REFERENCES

1. A. Daidouh, M. L. Veiga, and C. Pico, *J. Solid State Chem.* **130,** 28 (1997).
2. A. Daidouh, M. L. Veiga, and C. Pico, *Solid State Ionics* **106,** 103 (1998).
3. A. K. Jonscher, "Dielectric Relaxation Law." Chelsea Dielectric Press, London, 1996.
4. A. R. West, "Solid state Chemistry and Its Applications." Wiley, New York, 1990.
5. M. M. Borel, A. Leclaire, J. Chardon, J. Provost, and B. Raveau, *J. Solid State Chem.* **137,** 214 (1998).
6. S. T. Bramwell, A. M Buckley, and P. Day, *J. Solid State Chem.* **111,** 225 (1994).
7. B. Elouadi and L. Elammari, *Ferroelectrics* **107,** 253 (1990).
8. E. N. Matveinko, O. V. Yacubovich, M. A. Simonov, and N. V. Belov, *Dockl. Akad. Nauk SSSR* **259,** (1981); Sov. Phys. Dockl. **26,** 633, (1981).
9. R. Mackay, T. A. Wardojo, and S. Hwu, *J. Solid State Chem.* **125,** 225 (1996).
10. A. Daidouh, Tesis doctoral, Universidad Complutense de Madrid, Madrid, 1998.
11. J. Rodriguez-Carvajal, "Fullprof Program. III," Grenoble, France, 1994.
12. J. B. Goodenough, "Magnetism and Chemical Bond." Krieger, New York, 1976.
13. W. M. Reif, J. H. Zhang, and C. C. Torardi, *J. Solid State Chem.* **62**, 231 (1986).
14. K. Rissouli, K. Benkhouja, A. Sadel, M. Bettach, M. Zahir, M. Giorgi, M. Pierrot, and M. Drillon, *Eur. J. Solid State Inorg. Chem.* **34,** 221 (1997).
15. A. J. Heeger, O. Beekman, and A. M. Portis, *Phys Rev. B* **123** (5), 1652 (1961).
16. J. Fompeyrine, J. Darriet, J. J. Maguer, J. M. Ggrenech, G. Courbion, T. Roisnel, and J. Rodriguez-Carvajal, *J. Solid State Chem.* **131,** 198 (1997).
17. J. P. Attfield, A. K. Cheetham, D. C. Jhonson, and C. C. Torardi, *Inorg. Chem.* **26,** 3379 (1987).
18. J. P. Attfield, P. D. Battle, and A. K. Cheetman, *J. Solid State Chem.* **57,** 357 (1985).
19. M. A. G. Aranda, S. Bruque, J. P. Attfield, F. Palacio, and R. B. V. Dreele, *J. Solid State Chem.* **132,** 202 (1997).
20. D. Papoutsakis, J. E. Jackson, and D. G. Nocera, *Inorg. Chem.* **35,** 800 (1996).
21. T. Moriya, *Phys Rev.* **120**(1) 91 (1960).
22. W. M. Reif, J. H. Zhang, H. Tam, J. P. Attfield, and C. C. Torardi, *J. Solid State Chem.* **130,** 147 (1997).
23. P. W. Anderson, *Solid State Phys.* **14,** 99 (1963).
24. P. J. Hay, Thibeult, and R. Hoffmann, *J. Am. Chem. Soc.* **20,** 4884 (1975).